DESY 95-083
April 1995

Study of the Photon Remnant in Resolved Photoproduction at HERA

ZEUS Collaboration

Abstract

Photoproduction at HERA is studied in ep collisions, with the ZEUS detector, for γp centre-of-mass energies ranging from 130-270 GeV. A sample of events with two high-p_T jets ($p_T > 6$ GeV, $\eta < 1.6$) and a third cluster in the approximate direction of the electron beam is isolated using a clustering algorithm. These events are mostly due to resolved photoproduction. The third cluster is identified as the photon remnant. Its properties, such as the transverse and longitudinal energy flows around the axis of the cluster, are consistent with those commonly attributed to jets, and in particular with those found for the two jets in these events. The mean value of the photon remnant p_T with respect to the beam axis is measured to be 2.1 ± 0.2 GeV, which demonstrates substantial mean transverse momenta for the photon remnant.

The ZEUS Collaboration

M. Derrick, D. Krakauer, S. Magill, D. Mikunas, B. Musgrave, J. Repond, R. Stanek, R.L. Talaga, H. Zhang
Argonne National Laboratory, Argonne, IL, USA [p]

R. Ayad[1], G. Bari, M. Basile, L. Bellagamba, D. Boscherini, A. Bruni, G. Bruni, P. Bruni, G. Cara Romeo, G. Castellini[2], M. Chiarini, L. Cifarelli[3], F. Cindolo, A. Contin, M. Corradi, I. Gialas[4], P. Giusti, G. Iacobucci, G. Laurenti, G. Levi, A. Margotti, T. Massam, R. Nania, C. Nemoz, F. Palmonari, A. Polini, G. Sartorelli, R. Timellini, Y. Zamora Garcia[1], A. Zichichi
University and INFN Bologna, Bologna, Italy [f]

A. Bargende[5], J. Crittenden, K. Desch, B. Diekmann[6], T. Doeker, M. Eckert, L. Feld, A. Frey, M. Geerts, G. Geitz[7], M. Grothe, T. Haas, H. Hartmann, K. Heinloth, E. Hilger, H.-P. Jakob, U.F. Katz, S.M. Mari[4], A. Mass[8], S. Mengel, J. Mollen, E. Paul, Ch. Rembser, D. Schramm, J. Stamm, R. Wedemeyer
Physikalisches Institut der Universität Bonn, Bonn, Federal Republic of Germany [c]

S. Campbell-Robson, A. Cassidy, N. Dyce, B. Foster, S. George, R. Gilmore, G.P. Heath, H.F. Heath, T.J. Llewellyn, C.J.S. Morgado, D.J.P. Norman, J.A. O'Mara, R.J. Tapper, S.S. Wilson, R. Yoshida
H.H. Wills Physics Laboratory, University of Bristol, Bristol, U.K. [o]

R.R. Rau
Brookhaven National Laboratory, Upton, L.I., USA [p]

M. Arneodo[9], L. Iannotti, M. Schioppa, G. Susinno
Calabria University, Physics Dept.and INFN, Cosenza, Italy [f]

A. Bernstein, A. Caldwell, N. Cartiglia, J.A. Parsons, S. Ritz[10], F. Sciulli, P.B. Straub, L. Wai, S. Yang, Q. Zhu
Columbia University, Nevis Labs., Irvington on Hudson, N.Y., USA [q]

P. Borzemski, J. Chwastowski, A. Eskreys, K. Piotrzkowski, M. Zachara, L. Zawiejski
Inst. of Nuclear Physics, Cracow, Poland [j]

L. Adamczyk, B. Bednarek, K. Jeleń, D. Kisielewska, T. Kowalski, E. Rulikowska-Zarębska, L. Suszycki, J. Zając
Faculty of Physics and Nuclear Techniques, Academy of Mining and Metallurgy, Cracow, Poland [j]

A. Kotański, M. Przybycień
Jagellonian Univ., Dept. of Physics, Cracow, Poland [k]

L.A.T. Bauerdick, U. Behrens, H. Beier[11], J.K. Bienlein, C. Coldewey, O. Deppe, K. Desler, G. Drews, M. Flasiński[12], D.J. Gilkinson, C. Glasman, P. Göttlicher, J. Große-Knetter, B. Gutjahr[13], W. Hain, D. Hasell, H. Heßling, Y. Iga, P. Joos, M. Kasemann, R. Klanner, W. Koch, L. Köpke[14], U. Kötz, H. Kowalski, J. Labs, A. Ladage, B. Löhr, M. Löwe, D. Lüke, J. Mainusch, O. Mańczak, T. Monteiro[15], J.S.T. Ng, S. Nickel[16], D. Notz, K. Ohrenberg, M. Roco, M. Rohde, J. Roldán, U. Schneekloth, W. Schulz, F. Selonke, E. Stiliaris[17], B. Surrow, T. Voß, D. Westphal, G. Wolf, C. Youngman, J.F. Zhou
Deutsches Elektronen-Synchrotron DESY, Hamburg, Federal Republic of Germany

H.J. Grabosch, A. Kharchilava, A. Leich, M.C.K. Mattingly, A. Meyer, S. Schlenstedt, N. Wulff
DESY-Zeuthen, Inst. für Hochenergiephysik, Zeuthen, Federal Republic of Germany

G. Barbagli, P. Pelfer
University and INFN, Florence, Italy [f]

G. Anzivino, G. Maccarrone, S. De Pasquale, L. Votano
INFN, Laboratori Nazionali di Frascati, Frascati, Italy [f]

A. Bamberger, S. Eisenhardt, A. Freidhof, S. Söldner-Rembold[18], J. Schroeder[19], T. Trefzger
Fakultät für Physik der Universität Freiburg i.Br., Freiburg i.Br., Federal Republic of Germany [c]

N.H. Brook, P.J. Bussey, A.T. Doyle[20], J.I. Fleck[4], D.H. Saxon, M.L. Utley, A.S. Wilson
Dept. of Physics and Astronomy, University of Glasgow, Glasgow, U.K. [o]

A. Dannemann, U. Holm, D. Horstmann, T. Neumann, R. Sinkus, K. Wick
Hamburg University, I. Institute of Exp. Physics, Hamburg, Federal Republic of Germany [c]

E. Badura[21], B.D. Burow[22], L. Hagge, E. Lohrmann, J. Milewski, M. Nakahata[23], N. Pavel, G. Poelz, W. Schott, F. Zetsche
Hamburg University, II. Institute of Exp. Physics, Hamburg, Federal Republic of Germany [c]

T.C. Bacon, I. Butterworth, E. Gallo, V.L. Harris, B.Y.H. Hung, K.R. Long, D.B. Miller, P.P.O. Morawitz, A. Prinias, J.K. Sedgbeer, A.F. Whitfield
Imperial College London, High Energy Nuclear Physics Group, London, U.K. [o]

U. Mallik, E. McCliment, M.Z. Wang, S.M. Wang, J.T. Wu, Y. Zhang
University of Iowa, Physics and Astronomy Dept., Iowa City, USA [p]

P. Cloth, D. Filges
Forschungszentrum Jülich, Institut für Kernphysik, Jülich, Federal Republic of Germany

S.H. An, S.M. Hong, S.W. Nam, S.K. Park, M.H. Suh, S.H. Yon
Korea University, Seoul, Korea [h]

R. Imlay, S. Kartik, H.-J. Kim, R.R. McNeil, W. Metcalf, V.K. Nadendla
Louisiana State University, Dept. of Physics and Astronomy, Baton Rouge, LA, USA [p]

F. Barreiro[24], G. Cases, J.P. Fernandez, R. Graciani, J.M. Hernández, L. Hervás[24], L. Labarga[24], M. Martinez, J. del Peso, J. Puga, J. Terron, J.F. de Trocóniz
Univer. Autónoma Madrid, Depto de Física Teóríca, Madrid, Spain [n]

G.R. Smith
University of Manitoba, Dept. of Physics, Winnipeg, Manitoba, Canada [a]

F. Corriveau, D.S. Hanna, J. Hartmann, L.W. Hung, J.N. Lim, C.G. Matthews, P.M. Patel, L.E. Sinclair, D.G. Stairs, M. St.Laurent, R. Ullmann, G. Zacek
McGill University, Dept. of Physics, Montréal, Québec, Canada [a, b]

V. Bashkirov, B.A. Dolgoshein, A. Stifutkin
Moscow Engineering Physics Institute, Mosocw, Russia [l]

G.L. Bashindzhagyan, P.F. Ermolov, L.K. Gladilin, Y.A. Golubkov, V.D. Kobrin, V.A. Kuzmin, A.S. Proskuryakov, A.A. Savin, L.M. Shcheglova, A.N. Solomin, N.P. Zotov
Moscow State University, Institute of Nuclear Physics, Moscow, Russia [m]

M. Botje, F. Chlebana, A. Dake, J. Engelen, M. de Kamps, P. Kooijman, A. Kruse, H. Tiecke, W. Verkerke, M. Vreeswijk, L. Wiggers, E. de Wolf, R. van Woudenberg
NIKHEF and University of Amsterdam, Netherlands [i]

D. Acosta, B. Bylsma, L.S. Durkin, K. Honscheid, C. Li, T.Y. Ling, K.W. McLean[25], W.N. Murray, I.H. Park, T.A. Romanowski[26], R. Seidlein[27]
Ohio State University, Physics Department, Columbus, Ohio, USA [p]

D.S. Bailey, A. Byrne[28], R.J. Cashmore, A.M. Cooper-Sarkar, R.C.E. Devenish, N. Harnew, M. Lancaster, L. Lindemann[4], J.D. McFall, C. Nath, V.A. Noyes, A. Quadt, J.R. Tickner, H. Uijterwaal, R. Walczak, D.S. Waters, F.F. Wilson, T. Yip
Department of Physics, University of Oxford, Oxford, U.K. [o]

G. Abbiendi, A. Bertolin, R. Brugnera, R. Carlin, F. Dal Corso, M. De Giorgi, U. Dosselli, S. Limentani, M. Morandin, M. Posocco, L. Stanco, R. Stroili, C. Voci
Dipartimento di Fisica dell' Universita and INFN, Padova, Italy [f]

J. Bulmahn, J.M. Butterworth, R.G. Feild, B.Y. Oh, J.J. Whitmore[29]
Pennsylvania State University, Dept. of Physics, University Park, PA, USA [q]

G. D'Agostini, G. Marini, A. Nigro, E. Tassi
Dipartimento di Fisica, Univ. 'La Sapienza' and INFN, Rome, Italy [f]

J.C. Hart, N.A. McCubbin, K. Prytz, T.P. Shah, T.L. Short
Rutherford Appleton Laboratory, Chilton, Didcot, Oxon, U.K. [o]

E. Barberis, T. Dubbs, C. Heusch, M. Van Hook, B. Hubbard, W. Lockman, J.T. Rahn, H.F.-W. Sadrozinski, A. Seiden
University of California, Santa Cruz, CA, USA [p]

J. Biltzinger, R.J. Seifert, O. Schwarzer, A.H. Walenta, G. Zech
Fachbereich Physik der Universität-Gesamthochschule Siegen, Federal Republic of Germany [c]

H. Abramowicz, G. Briskin, S. Dagan[30], A. Levy[31]
School of Physics, Tel-Aviv University, Tel Aviv, Israel [e]

T. Hasegawa, M. Hazumi, T. Ishii, M. Kuze, S. Mine, Y. Nagasawa, M. Nakao, I. Suzuki, K. Tokushuku, S. Yamada, Y. Yamazaki
Institute for Nuclear Study, University of Tokyo, Tokyo, Japan [g]

M. Chiba, R. Hamatsu, T. Hirose, K. Homma, S. Kitamura, Y. Nakamitsu, K. Yamauchi
Tokyo Metropolitan University, Dept. of Physics, Tokyo, Japan [g]

R. Cirio, M. Costa, M.I. Ferrero, L. Lamberti, S. Maselli, C. Peroni, R. Sacchi, A. Solano, A. Staiano
Universita di Torino, Dipartimento di Fisica Sperimentale and INFN, Torino, Italy [f]

M. Dardo
II Faculty of Sciences, Torino University and INFN - Alessandria, Italy [f]

D.C. Bailey, D. Bandyopadhyay, F. Benard, M. Brkic, M.B. Crombie, D.M. Gingrich[32], G.F. Hartner, K.K. Joo, G.M. Levman, J.F. Martin, R.S. Orr, C.R. Sampson, R.J. Teuscher
University of Toronto, Dept. of Physics, Toronto, Ont., Canada [a]

C.D. Catterall, T.W. Jones, P.B. Kaziewicz, J.B. Lane, R.L. Saunders, J. Shulman
University College London, Physics and Astronomy Dept., London, U.K. [o]

K. Blankenship, B. Lu, L.W. Mo
Virginia Polytechnic Inst. and State University, Physics Dept., Blacksburg, VA, USA [q]

W. Bogusz, K. Charchuła, J. Ciborowski, J. Gajewski, G. Grzelak, M. Kasprzak, M. Krzyżanowski, K. Muchorowski, R.J. Nowak, J.M. Pawlak, T. Tymieniecka, A.K. Wróblewski, J.A. Zakrzewski, A.F. Żarnecki
Warsaw University, Institute of Experimental Physics, Warsaw, Poland [j]

M. Adamus
Institute for Nuclear Studies, Warsaw, Poland [j]

Y. Eisenberg[30], U. Karshon[30], D. Revel[30], D. Zer-Zion
Weizmann Institute, Nuclear Physics Dept., Rehovot, Israel [d]

I. Ali, W.F. Badgett, B. Behrens, S. Dasu, C. Fordham, C. Foudas, A. Goussiou, R.J. Loveless, D.D. Reeder, S. Silverstein, W.H. Smith, A. Vaiciulis, M. Wodarczyk
University of Wisconsin, Dept. of Physics, Madison, WI, USA [p]

T. Tsurugai
Meiji Gakuin University, Faculty of General Education, Yokohama, Japan

S. Bhadra, M.L. Cardy, C.-P. Fagerstroem, W.R. Frisken, K.M. Furutani, M. Khakzad, W.B. Schmidke
York University, Dept. of Physics, North York, Ont., Canada [a]

[1] supported by Worldlab, Lausanne, Switzerland
[2] also at IROE Florence, Italy
[3] now at Univ. of Salerno and INFN Napoli, Italy
[4] supported by EU HCM contract ERB-CHRX-CT93-0376
[5] now at Möbelhaus Kramm, Essen
[6] now a self-employed consultant
[7] on leave of absence
[8] now at Institut für Hochenergiephysik, Univ. Heidelberg
[9] now also at University of Torino
[10] Alfred P. Sloan Foundation Fellow
[11] presently at Columbia Univ., supported by DAAD/HSPII-AUFE
[12] now at Inst. of Computer Science, Jagellonian Univ., Cracow
[13] now at Comma-Soft, Bonn
[14] now at Univ. of Mainz
[15] supported by DAAD and European Community Program PRAXIS XXI
[16] now at Dr. Seidel Informationssysteme, Frankfurt/M.
[17] supported by the European Community
[18] now with OPAL Collaboration, Faculty of Physics at Univ. of Freiburg
[19] now at SAS-Institut GmbH, Heidelberg
[20] also supported by DESY
[21] now at GSI Darmstadt
[22] also supported by NSERC
[23] now at Institute for Cosmic Ray Research, University of Tokyo
[24] partially supported by CAM
[25] now at Carleton University, Ottawa, Canada
[26] now at Department of Energy, Washington
[27] now at HEP Div., Argonne National Lab., Argonne, IL, USA
[28] now at Oxford Magnet Technology, Eynsham, Oxon
[29] on leave and partially supported by DESY 1993-95
[30] supported by a MINERVA Fellowship
[31] partially supported by DESY
[32] now at Centre for Subatomic Research, Univ.of Alberta, Canada and TRIUMF, Vancouver, Canada

[a] supported by the Natural Sciences and Engineering Research Council of Canada (NSERC)
[b] supported by the FCAR of Québec, Canada
[c] supported by the German Federal Ministry for Research and Technology (BMFT)
[d] supported by the MINERVA Gesellschaft für Forschung GmbH, and by the Israel Academy of Science
[e] supported by the German Israeli Foundation, and by the Israel Academy of Science
[f] supported by the Italian National Institute for Nuclear Physics (INFN)
[g] supported by the Japanese Ministry of Education, Science and Culture (the Monbusho) and its grants for Scientific Research
[h] supported by the Korean Ministry of Education and Korea Science and Engineering Foundation
[i] supported by the Netherlands Foundation for Research on Matter (FOM)
[j] supported by the Polish State Committee for Scientific Research (grant No. SPB/P3/202/93) and the Foundation for Polish- German Collaboration (proj. No. 506/92)
[k] supported by the Polish State Committee for Scientific Research (grant No. PB 861/2/91 and No. 2 2372 9102, grant No. PB 2 2376 9102 and No. PB 2 0092 9101)
[l] partially supported by the German Federal Ministry for Research and Technology (BMFT)
[m] supported by the German Federal Ministry for Research and Technology (BMFT), the Volkswagen Foundation, and the Deutsche Forschungsgemeinschaft
[n] supported by the Spanish Ministry of Education and Science through funds provided by CICYT
[o] supported by the Particle Physics and Astronomy Research Council
[p] supported by the US Department of Energy
[q] supported by the US National Science Foundation

1 Introduction

Hard scattering between a real photon and a proton is expected, in lowest order QCD, to occur by two different mechanisms (Fig. 1). The photon may interact directly with a quark or gluon from the proton or it may resolve into its constituent quarks and gluons which then interact with the partons from the proton. These two processes are called direct and resolved photoproduction, respectively [1].

In direct photoproduction, the entire photon participates in the hard scatter. In resolved photoproduction on the other hand, only a fraction of the momentum of the photon is involved in the hard scatter while the remaining momentum is carried by spectator partons. These partons fragment into a photon remnant which is expected to be approximately collinear with the original photon. The presence of resolved photon interactions at HERA has been demonstrated [2, 3] and the existence of the photon remnant has been confirmed. The separation between the direct and resolved contributions has also been reported, together with the measurement of a differential dijet cross section [4]. Inclusive jet [5, 6] and dijet [7] cross sections have given further information on the kinematic properties of these two processes and on the gluon content of the proton as well as on the parton structure of the photon.

The presence of a photon remnant in photon-proton collisions has been used as a means to identify resolved photoproduction interactions. The study of the photon remnant itself, however, is also interesting: a detailed comparison with leading-order (LO) predictions has not been performed and little is known about the internal structure of the photon remnant. On the theoretical side, although the point-like coupling of the photon to quark-antiquark pairs is included in parameterizations of the photon structure function, most Monte Carlo simulations model the resolved photon as a hadron, with collinear incoming partons. This results in a photon remnant with low-p_T with respect to the beam axis. Several studies have suggested that next-to-leading-order contributions or fluctuations of the photon into quark-antiquark pairs with high virtuality may lead to a 'photon remnant' which has sizable transverse momentum with respect to the incident photon direction [8, 9, 10].

In this paper, the photon remnant is isolated for the first time. Its properties are studied using a clustering algorithm and are found to be consistent with those commonly attributed to jets. These remnant jets are then compared with the jets emerging from the hard interaction and with LO Monte Carlo expectations. The data were collected with the ZEUS detector during the 1993 data-taking period. The study is conducted for γp centre-of-mass energies ($W_{\gamma p}$) in the range $130 < W_{\gamma p} < 270$ GeV.

2 Experimental setup

Details of the ZEUS detector have been described elsewhere [11]. The primary components used in this analysis are the calorimeter and the tracking detectors. The uranium-scintillator calorimeter [12] covers 99.7% of the total solid angle. It is subdivided into electromagnetic and hadronic sections with cell sizes of 5×20 cm^2 (10×20 cm^2 in the outgoing electron direction[1]) and 20×20 cm^2, respectively. It consists of three parts: the rear calorimeter (RCAL) covering the region $-3.8 < \eta < -0.75$, the barrel calorimeter (BCAL) covering the region $-0.75 < \eta < 1.1$ and the forward calorimeter (FCAL) covering the region $1.1 < \eta < 4.3$.

[1]The Z axis is defined to lie along the proton direction; the Y axis points upward; the pseudorapidity, $\eta = -\ln(\tan\frac{\theta}{2})$ where θ is the angle with respect to the Z axis.

The calorimeter has an energy resolution achieved in test beams of $\sigma/E = 18(35)\ \%/\sqrt{E(\mathrm{GeV})}$ for electrons (hadrons). The timing resolution for each cell is $\sigma_t = 1.5/\sqrt{E} \oplus 0.5$ ns, where E (GeV) is the energy deposited in the cell.
The tracking system consists of a vertex detector [13] and a central tracking chamber [14] inside a 1.43 T solenoidal magnetic field. The interaction vertex is measured with a resolution along (transverse to) the beam direction of 0.4 (0.1) cm.
The luminosity is measured, using the electron-proton bremsstrahlung process, by electron and photon lead-scintillator calorimeters [15] installed inside the HERA tunnel. In 1993 the beam energies at HERA were $E_e = 26.7$ GeV for the electrons and $E_p = 820$ GeV for the protons. Typical electron and proton currents were about 10 mA and the instantaneous luminosity was about 6×10^{29} cm^{-2} s^{-1}. HERA operated with 84 colliding bunches. Additional electron and proton bunches circulated without colliding and are used for background measurements.

3 Trigger and data selection

In this analysis, photoproduction events are defined by requiring that the electron was scattered at small angles and was not detected in the calorimeter. This requirement corresponds approximately to a cut of $Q^2 \leq 4$ GeV^2, giving a median Q^2 of about 10^{-3} GeV^2 [4]. The trigger selects hard scattering events at low Q^2.
The ZEUS detector uses a three level trigger [11]. In the first level trigger, the calorimeter cell energies were combined to define regional and global sums which were required to exceed given thresholds [16]. The second level trigger mainly rejected beam-gas interactions using timing information from the calorimeter. The third level trigger performed further rejection of beam-gas and cosmic ray events using information from both the calorimeter and the tracking chambers. An event was rejected if no vertex was found by the central tracking chambers or if the vertex was located in the region $|Z| > 75$ cm. To reject beam-gas interactions, events were selected based on the following kinematic cuts [6]: $E_{tot} - p_Z \geq 8$ GeV, $p_Z/E_{tot} \leq 0.94$ and $E_T^{cone} \geq 12$ GeV, where the calorimetric quantities E_{tot}, p_Z and E_T^{cone} are the total energy, the total longitudinal energy and the transverse energy excluding a cone of 10° in the forward direction, respectively. About 470,000 triggers were collected with these trigger conditions.
As in previous studies of hard photoproduction [6, 7], the following offline cuts were applied to select the final event sample.

- Beam-gas interactions were reduced by tightening calorimeter timing cuts, as well as cuts on the correlation between the vertex position (defined by the tracking chambers) and the calorimeter timing [17].
- The E_T^{cone} cut was raised to $E_T^{cone} \geq 15$ GeV to select hard scattering events.
- To reduce beam-gas interactions, the event was rejected if less than 10% of the tracks pointed toward the vertex.
- Deep inelastic scattering (DIS) neutral current events were removed from the sample as described in our previous publications [2, 4].
- The fraction of the initial electron energy carried by the almost real photon, $y = E_\gamma/E_e$ where E_γ is the photon energy, was measured using the Jacquet-Blondel [18] estimator

of the Bjorken-y:

$$y_{JB} = \frac{\Sigma_i (E^i - p_Z^i)}{2E_e}.$$

The sum runs over calorimeter cells with energy E^i and longitudinal energy p_Z^i. To reduce uranium noise, the cell energies were required to be greater than 60 MeV (110 MeV) for the electromagnetic (hadronic) cells. This calculation assumes that the scattered electron was not detected in the calorimeter. For DIS events in which the electron deposits energy but is not identified in the calorimeter, y_{JB} will be near unity. Therefore, for further rejection of DIS events, we required $y_{JB} < 0.7$. To reject proton-gas interactions, $y_{JB} \geq 0.2$ was required. These requirements correspond approximately to $0.2 < y < 0.85$.

- To remove charged current background and cosmic ray showers, a cut on $\not\!\!p_T/\sqrt{E_T} < 1.5$ GeV$^{1/2}$ was imposed, where $\not\!\!p_T$ is the total transverse momentum and E_T is the total transverse energy of the event.

After these selection cuts, a sample of 99,894 events remained, corresponding to an integrated luminosity of 0.55 pb^{-1}. The estimated proton-gas and DIS background contributions are 0.4% and 1 to 2%, respectively. Cosmic ray and electron-gas backgrounds are negligible.

4 Monte Carlo simulation

In the following, the data are compared to Monte Carlo simulations based on the PYTHIA 5.6 [19] event generator which includes leading-order QCD calculations. The HERWIG 5.7 [20] event generator was used to check the PYTHIA results. The cut on the minimum transverse momentum, $\hat{p}_{Tmin}$, of a hard scatter was set at 2.5 GeV. In PYTHIA, the photon flux is calculated using the Weizsäcker-Williams approximation. The parton densities used were GRV LO [21] for the photon and MRSD$_-$ [22] for the proton. For comparison, we also used the parameterization LAC1 [23] for the photon.
The generated events were passed through a detector simulation based on GEANT 3.13 [24]. The same reconstruction program that was used in the data analysis was applied to the generated events. The generated Monte Carlo event sample was obtained by combining the resolved and direct samples in proportion to the generated Monte Carlo cross sections (approximately 7:1 for the GRV photon parton densities).
In PYTHIA the distribution of the intrinsic transverse momentum, k_t, of the partons in the proton and in the resolved photon is parameterized by the distribution, $dN/dk_t^2 \propto e^{-k_t^2/k_0^2}$, where k_0 is a parameter which determines the hardness of the k_t spectrum. The default value of k_0 for both the proton and the resolved photon is 0.44 GeV. An option in PYTHIA allows events to be generated using a different functional form for the k_t spectrum and a different value of k_0. This option has been used to generate events with a harder k_t spectrum (see section 8).

5 Analysis using the $k_\perp$ algorithm

Previous analyses of photoproduction at HERA have implemented a cone algorithm to find jets [2, 3, 4]. This algorithm [25] uses a cone of fixed radius in pseudorapidity and azimuthal angle space and maximizes the transverse energy within this cone. It is therefore well suited for high transverse energy jets. The photon remnant, however, is expected to deposit energy in the electron direction with low transverse energy. Due to the rapid variation of pseudorapidity

in this region, and to the low transverse energy, a cone algorithm cannot be used to identify the photon remnant. Therefore, we chose to use the $k_\perp$ clustering algorithm [26]. The analysis was done in the laboratory frame instead of the γp frame due to the uncertainties in the boost. The $k_\perp$ algorithm finds jets by iteratively merging clusters. Initially, clusters are individual calorimeter cells. For the Monte Carlo events, the algorithm is also used to cluster generated particles (see section 7). In the merging procedure, the quantity $k_\perp$ is evaluated for each pair of clusters,

$$k_\perp = 2E^2_{min}(1 - \cos\theta_{nm}),$$

where θ_{nm} is the angle between the two clusters n and m, and E_{min} is the minimum value of the cluster energies E_n and E_m. In the small angle approximation, $k_\perp$ is the transverse momentum squared of the lower energy cluster with respect to the higher energy cluster. A pseudo-particle with infinite momentum along the Z axis is included in the clustering procedure to take the proton remnant into account. The value of $k_\perp$ between the pseudo-particle and the other clusters is calculated using the same formula as above. When all of the $k_\perp$ values have been calculated, the two clusters with the lowest $k_\perp$ value are merged. The four-momentum of the new cluster is the sum of the four-momenta of the two merged clusters. The calculation of $k_\perp$ is then repeated, replacing the two merged clusters with the new cluster. The iteration continues until the energy-angle resolution variable, Y (Y $= k_\perp/E_T^2$, where E_T is the total event energy transverse to the beam axis), becomes larger than some threshold, Y_{cut}. The value of Y_{cut} may be fixed or chosen on an event-by-event basis. For high transverse energy jets, the $k_\perp$ cluster-finding algorithm gives results which are similar to those obtained with the cone algorithm.

6 Photon remnant identification

To identify the photon remnant, we begin with an intuitive approach which is later justified using simulated events. As illustrated by Fig. 1b, resolved hard photoproduction events have a final state which includes two high p_T jets from the hard scatter as well as photon and proton remnants. Since we expect to find three clusters (in addition to the proton remnant) in each event, we choose the value of Y_{cut} on an event-by-event basis so that three clusters are found in each event [27]. These three clusters then should correspond to the two clusters from the hard scatter and the photon remnant. Since the photon remnant is expected to have low transverse momentum with respect to the beam axis, the separation between the photon remnant and the two jets from the hard scatter can be achieved, to a first approximation, by associating the photon remnant with the cluster having the smallest transverse momentum. For direct events, where we do not expect to see a photon remnant, the lowest transverse momentum cluster will either be part of the proton remnant or part of one of the two high transverse momentum jets. Therefore, the pseudorapidity distributions of the lowest transverse momentum clusters will be different for resolved and direct events.

In Fig. 2a-c, we show the (uncorrected) pseudorapidity distributions of the three clusters obtained with the $k_\perp$ algorithm. The data (full circles) and Monte Carlo events (histogram) are shown normalized in the region $\eta^{cal} \leq 1.6$. While the two clusters with the highest ${p_T}^{cal}$ (Fig. 2a,b) are mostly found in the $\eta^{cal} > 0$ region, the third cluster, with the lowest ${p_T}^{cal}$, (Fig. 2c) is observed mostly in the $\eta^{cal} < 0$ region, *i.e.* in the photon direction. Data and Monte Carlo expectations agree for the two highest ${p_T}^{cal}$ clusters except in the forward region, $\eta^{cal} > 1.6$, where we observe, in the data, an excess similar to that already reported in our previous anal-

yses [6, 7]. The peak observed in Fig. 2c, for the third cluster, in the negative pseudorapidity region is accounted for by the Monte Carlo simulation including resolved and direct processes (full histogram). The Monte Carlo distribution, however, is shifted slightly to lower values. The direct process, which does not contain a photon remnant, does not contribute to this peak as shown by the dashed line in the figure. Therefore, we are justified in using this method to separate direct and resolved events. In addition, the third cluster, when it is in the negative pseudorapidity region, can be associated with the photon remnant.

In order to maximize the possibility that the two highest ${p_T}^{cal}$ clusters stem from the partons in the hard scatter and to minimize the possibility that one of the two highest ${p_T}^{cal}$ clusters is, in fact, part of the proton remnant, we require that the two highest ${p_T}^{cal}$ clusters have high transverse momentum ($p_{T\,1,2}^{cal} > 5$ GeV) and that they are well separated from the forward region ($\eta_{1,2}^{cal} < 1.6$).

The distribution of the pseudorapidity of the third cluster, η_3^{cal}, after the above cuts and the requirement $E_3^{cal} > 2$ GeV, is shown in Fig. 2d. The comparison with the distribution predicted for direct processes shows that the events with $\eta_3^{cal} < -1$ are almost exclusively due to resolved processes. The agreement of the Monte Carlo simulation for resolved plus direct contributions with the data is not perfect; in the data there are somewhat fewer events with large negative η_3^{cal} values. The difference between the data and the Monte Carlo simulation is not improved when the photon parton parameterization LAC1 (dotted line) is used instead of GRV LO. For the following analysis, the resolved event sample is selected by requiring $\eta_3^{cal} < -1$.

A measurement of the mean value of Y_{cut} also demonstrates the difference between the two event samples on either side of $\eta_3^{cal} = -1$. Higher values of Y_{cut} indicate energetic clusters which are spatially well separated. For the events at high η_3^{cal}, the mean value of Y_{cut} is 0.028. For the low η_3^{cal} events, the mean value of Y_{cut} is 0.063. This result suggests that the high η_3^{cal} events contain a significant number of direct, two-jet events, for which the clustering procedure has been prematurely stopped. For the sample at $\eta_3^{cal} < -1$, however, the separation between the three clusters is quite distinct.

A total of 1370 events satisfy the cuts. For these events, the fraction of the photon momentum involved in the hard scattering, x_γ, measured from the two highest p_T^{cal} jets [4], peaks at low values as expected for resolved processes (not shown). By defining direct events, in this sample, as events with $x_\gamma > 0.75$ [7], we obtain a contribution from direct processes of about 8%. The contribution from direct photon interactions, estimated using LO direct Monte Carlo events, is also 8%.

7 Correction procedure

In the following, the data are corrected back to the hadron level using the PYTHIA Monte Carlo program previously described. For the Monte Carlo events, the $k_\perp$ algorithm is applied independently at both the generated hadron level and the calorimeter cell level. In both cases the resulting clusters are sorted according to p_T. The detector level cuts in η^{cal}, ${p_T}^{cal}$, E_3^{cal}, and y_{JB} correspond approximately to two hadron jets with $p_{T\,1,2} > 6.0$ GeV and $\eta_{1,2} < 1.6$, a remnant cluster with $\eta_3 < -1$ and $E_3 > 2$ GeV, and $0.2 < y < 0.85$. Therefore, the hadron level Monte Carlo distributions were determined for events within this kinematic region.

The correspondence between hadron and calorimeter clusters was determined by comparing the value of $k_\perp$ for each pair of hadron and calorimeter clusters. Each hadron cluster was then matched with that calorimeter cluster with which it had the lowest value of $k_\perp$. After all cuts were applied at both the hadron and calorimeter levels, and neglecting the possible interchange

of the labels, cluster 1 and cluster 2, due to the sorting (this occurs in events in which the two highest p_T jets have similar p_T), all three clusters were found to be correctly matched for 97% of the events. For 3% of the events, a high-p_T cluster at one level was associated with the proton remnant at the other level. In less than 0.5% of the events, the lowest p_T clusters at the hadron and calorimeter levels were not matched.
The experimental shifts and resolutions of the measured variables were evaluated using the matched hadron and calorimeter clusters. The average measured value of η is shifted, with respect to the hadron level, by less than $-0.02(+0.08)$ and has a resolution of 0.07(0.43) units for the first two jets (third cluster). The measured transverse jet momentum, with respect to the beam, is reduced, on average, by 15% and has a resolution of 11%. This is due either to the magnetic field acting on low energy particles or to dead material in the apparatus. The value of y is reconstructed with an average shift of -0.14 units and a resolution of 10%, also due to losses in the beam pipe and detector effects.
On average, the third cluster contains $75 \pm 20\%$ of the photon remnant energy, as defined by the third cluster energy at the hadron level. Inactive material in front of the calorimeter results in an energy loss of about 20%, independent of the cluster energy. Particles lost in the beam pipe account for the rest of the energy loss; this effect increases with cluster energy, becoming comparable to the detector effects at measured energies above 10 GeV.
The data were corrected with the following procedure. First, the contamination from events outside the kinematic range was estimated using Monte Carlo events and was subtracted bin-by-bin from the measured distributions. The resulting distributions were then corrected with a correlation matrix that was generated using the matched hadron and calorimeter clusters. The unfolding procedure is described in [28] and includes acceptance corrections for the trigger and cuts described in section 3. The statistical errors were estimated by randomly varying, within their statistical errors, both the experimental data (before the background subtraction) and the Monte Carlo correlation matrix and calculating the root mean squared deviation in each bin.
The systematic uncertainties were estimated by considering the following effects: different photon parton densities, a 5% energy scale uncertainty in the Monte Carlo simulation of the energy response of the calorimeter, a variation of the cuts on the measured quantities ($y_{_{JB}}$, $p_{T\,1,2}^{cal}$, $\eta_{1,2}^{cal}$, η_3^{cal}), corrections using the HERWIG Monte Carlo simulation, an increase in the direct cross section by a factor of three relative to the resolved one, and the use of calorimeter islands (see next section) instead of cells. For the HERWIG systematic study, a fraction of the events was generated with $\hat{p}_{Tmin}$ set to 5.0 GeV. The systematic errors were evaluated by calculating the root mean squared deviation between the original data point and each of the points found using the systematic variations mentioned above, weighting each deviation by its statistical errors. In the following figures the statistical errors are shown as the inner error bars; the outer bars show the statistical and systematic uncertainties added in quadrature.

8 Photon remnant properties

In Fig. 3, we show the pseudorapidity, transverse momentum (with respect to the Z axis), and energy distributions for the photon remnant, corrected back to the hadron level. The average correction factors are typically 1.2 and are approximately constant for each of the three variables.
The η_3 distribution is shown in Fig. 3a. The corrected data and the expectations from PYTHIA (solid histogram) disagree in the negative η_3 region, as observed in Fig. 2d. The measured

distribution peaks at higher values of η_3 than the Monte Carlo prediction. A similar effect can be observed in the transverse momentum distribution (Fig. 3b), where the requirement $\eta_3 < -1$ is applied for this and all following figures. Here also, the data show a higher average value. The distribution peaks at 1.5 GeV with a tail extending to 6 GeV. The mean value of the photon remnant p_T at the hadron level is measured to be $\langle p_{T3} \rangle = 2.1 \pm 0.2$ GeV. The Monte Carlo expectation is $\langle p_{T3} \rangle = 1.44 \pm 0.02$ GeV.

The energy distribution (Fig. 3c) peaks around 7 GeV and extends to 20 GeV. The solid histogram shows the Monte Carlo expectation which agrees with the data, except in the lowest bin where the Monte Carlo expectation is about 30% higher.

The unlikely possibility has been studied that an incorrect Monte Carlo description of the energy response in the RCAL might result in the observed discrepancy between the data and the Monte Carlo expectation. The RCAL energy scale was reduced by 10% within 10° of the RCAL beam pipe to simulate additional inactive material. The discrepancy in the p_{T3} distribution was not improved, and the disagreement with the data for the E_3 distribution became worse.

The observation that the average transverse momenta of the photon remnant is higher than expected from PYTHIA, is in qualitative agreement with the theoretical predictions mentioned in the introduction. Therefore, following [10], we have compared the data with Monte Carlo events generated with a harder intrinsic transverse momentum spectrum for the partons in the photon, *i.e.* $dN/dk_t^2 \propto 1/(k_t^2 + k_0^2)$. The "PYTHIA high k_t" results are shown as the dotted histograms in Fig. 3. The parameter k_0 is determined by minimizing the χ^2 between the Monte Carlo hadron level and the corrected data p_{T3} distributions. The result is $k_0 = 0.66 \pm 0.22$ GeV. This corresponds to $\langle k_t \rangle \approx 1.7$ GeV, as compared to 0.4 GeV for PYTHIA with default parameters. The agreement with the energy distribution is unchanged, while it is considerably improved for the η_3 and p_{T3} distributions. On the other hand, the distributions for the first two clusters remain unchanged (not shown). Equally good agreement between the data and the Monte Carlo simulation has been achieved by reweighting the Monte Carlo events to the default intrinsic k_t spectrum (not shown). In this case, $k_0 = 1.90 \pm 0.21$ GeV, much higher than the default value of $k_0 = 0.44$ GeV assumed in PYTHIA. These results show that adjusting the intrinsic transverse momenta of the partons in the photon is a way to improve the agreement between the data and the Monte Carlo predictions.

One of the well-known properties of jets is that the average energy transverse to the jet axis is limited as the jet energy increases. In general, this results in an average energy transverse to the jet axis per particle, $\langle E_T^i \rangle$, of the order of a few hundred MeV. In measuring this quantity for the photon remnant, we used calorimeter islands. Islands are groups of calorimeter cells more closely related to particles than individual calorimeter cells and therefore represent a better choice for this measurement. The analysis performed with calorimeter cells provides an upper limit on the systematic uncertainties of this measurement. Figure 4a shows the average value of $\langle E_T^i \rangle$ versus the cluster energy for the third cluster, both for the data after corrections and for the Monte Carlo simulation. The corrections include the effect of particles lost down the beam pipe. The largest component of the systematic errors (+30%) comes from using calorimeter cells instead of islands.

The mean value of $\langle E_T^i \rangle$ starts below 200 MeV, and slowly increases with the remnant energy, E_3. The total cluster energy, on the other hand, spans a range from 3 to 21 GeV. This result demonstrates that the photon remnant exhibits limited transverse energy per particle, as expected for jet-like objects. Further support to this conclusion is given in Fig. 4b, which shows the average values of the corrected total transverse ($\Sigma_i E_T^i$) and total longitudinal ($\Sigma_i E_L^i$) energy of the third cluster, with respect to the cluster axis, as a function of the energy of the

cluster. The longitudinal component increases much faster than the transverse energy, and most of the cluster energy is along the cluster axis. This is consistent with a jet-like structure of the photon remnant.
We also studied how the energy is distributed around the axis of the third cluster. Figure 4c shows the corrected energy flow of the third cluster as a function of $1 - \cos\Theta$ for both the data and the Monte Carlo simulation. Here, Θ is the angle of the particle with respect to the cluster axis. This is effectively a plot of the energy deposited in rings of fixed area centred on the cluster axis. Because there is not a simple correspondence between particles and calorimeter cells, it is difficult to construct a correlation matrix between the generated (hadron energy) and experimental (calorimeter cell energy) quantities. Therefore, these distributions are corrected bin-by-bin. The average correction factor is around 1.15. In Fig. 4c, we have required reconstructed (uncorrected) jet energies between 8 and 14 GeV and hadron level jet energies between 8 and 15 GeV. The statistical errors are the error on the mean. The energy distribution for the data is quite collimated. The Monte Carlo simulation agrees very well with the data, indicating that the fragmentation of the remnant is understood.

9 Comparison of the photon remnant with jets from hard scattering

Having established the jet-like properties of the photon remnant, we next compare it with the jets originating from parton hard scattering. The comparison of these two types of jets is of interest because one is the debris of the photon and is a low-p_T jet, with p_T typically well below 6 GeV, while the other two jets come from the hard scattering of the partons in the photon and proton and are high-p_T jets, with a minimum p_T of 6 GeV. A comparison between low-p_T and high-p_T jets has been proposed as a method of studying the hadronization process [29].
Figures 4d, e, and f present the results of this comparison for the average value of $\langle E_T^i \rangle$, $\langle \Sigma_i E_T^i \rangle$ and $\langle \Sigma_i E_L^i \rangle$, and $1-\cos\Theta$, respectively. In Fig. 4f, we again require reconstructed (uncorrected) jet energies between 8 and 14 GeV, and hadron level jet energies between 8 and 15 GeV. This cut is especially important for this figure in order to compare jets with approximately equal energies. In all figures, good agreement between the third cluster and the two hard jets is observed. From these comparisons we conclude that, in the kinematic region and for the variables studied, the low-p_T photon remnant jet exhibits the same hadronization characteristics as the high-p_T jets originating from the hard scattering process.

10 Conclusions

For the first time, in a sample of quasi-real photon-proton collisions, the photon remnant produced in resolved photon interactions has been isolated. The selected events contain two high-p_T jets with $p_T > 6$ GeV and $\eta < 1.6$, and $130 < W_{\gamma p} < 270$ GeV. The properties of the photon remnant, as defined by a cluster with $\eta_3 < -1$ and $E_3 > 2$ GeV, are studied and shown to exhibit a collimated energy flow with a limited transverse energy with respect to the cluster axis, characteristic of a jet structure.
The leading order QCD Monte Carlo simulation, with default parameters, does not reproduce the pseudorapidity distribution or the transverse momentum distribution (with respect to the incident photon) of the photon remnant. The mean value of p_T for the photon remnant, 2.1 ± 0.2 GeV, is substantially larger than the Monte Carlo expectation. Better agreement can

be obtained by increasing the average intrinsic transverse momenta of the partons in the photon to about 1.7 GeV. These results are in qualitative agreement with theoretical expectations of substantial mean transverse momenta for the photon remnant.
The photon remnant has also been compared, in the laboratory frame, with the two high-p_T jets originating from the parton hard scattering. Although the origins of these two types of jets may be quite different, within the present statistics and in the kinematic range studied, they exhibit similar properties for the energy flow and the transverse and longitudinal energy with respect to the jet axis.

11 Acknowledgements

We thank the DESY directorate for their strong support and encouragement. The remarkable achievements of the HERA machine group were essential for the successful completion of this work, and are gratefully appreciated. We also gratefully acknowledge the support of the DESY computing and network services.

References

[1] J. F. Owens, Phys. Rev. D21 (1980) 54;
M. Drees and F. Halzen, Phys. Rev. Lett. 61 (1988) 275;
M. Drees and R. M. Godbole, Phys. Rev. D39 (1989) 169;
G. A. Schuler and T. Sjöstrand, Phys. Lett B300 (1993) 169.

[2] ZEUS Collab., M. Derrick et al., Phys. Lett. B297 (1992) 404.

[3] H1 Collab., T. Ahmed et al., Phys. Lett. B297 (1992) 205.

[4] ZEUS Collab., M. Derrick et al., Phys. Lett. B322 (1994) 287.

[5] H1 Collab., I. Abt et al., Phys. Lett. B314 (1993) 436.

[6] ZEUS Collab., M. Derrick et al., Phys. Lett. B342 (1995) 417.

[7] ZEUS Collab., M. Derrick et al., Phys. Lett. B348 (1995) 665.

[8] G. A. Schuler and T. Sjöstrand, preprint CERN-TH 7193/94.

[9] J. Chýla, Phys. Lett. B320 (1994) 186.

[10] M. Drees, Proceedings of the Aspen conference on Multiparticle Dynamics, Aspen, Colorado 1993 p. 110 and preprint MAD/PH/797.

[11] ZEUS Collab., The ZEUS Detector, Status Report (1993).

[12] M. Derrick et al., Nucl. Instr. Meth. A309 (1991) 77;
A. Andresen et al., Nucl. Instr. Meth. A309 (1991) 101;
A. Bernstein et al., Nucl. Instr. Meth. A336 (1993) 23.

[13] C. Alvisi et al., Nucl. Instr. Meth. A305 (1991) 30.

[14] B. Foster et al., Nucl. Phys. B, Proc. Suppl. B32 (1993) 181.

[15] J. Andruszków et al., DESY 92-066 (1992).

[16] W. H. Smith et al., Nucl. Instr. Meth. A355 (1995) 278.

[17] ZEUS Collab., M. Derrick et al., Phys. Lett. B316 (1993) 412.

[18] F. Jacquet and A. Blondel, Proc. of the Study for an *ep* Facility for Europe, ed. U. Amaldi, DESY 79/48 (1979) 391.

[19] H. U. Bengtsson and T. Sjöstrand, Comp. Phys. Comm, 46 (1987) 43; T. Sjöstrand, CERN-TH 6488/92.

[20] G. Marchesini et al., Comp. Phys. Comm. 67 (1992) 465.

[21] M. Glück, E. Reya and A. Vogt, Phys. Rev. D46 (1992) 1973.

[22] A. D. Martin, W. J. Stirling and R. G. Roberts, Phys. Rev. D47 (1993) 867.

[23] H. Abramowicz, K. Charchuła and A. Levy, Phys. Lett. B269 (1991) 458.

[24] R. Brun et al., GEANT3.13, CERN DD/EE/84-1 (1987).

[25] UA1 Collab., G. Arnison et al., Phys. Lett. B123 (1983) 115;
J. E. Huth et al., FERMILAB-Conf-90-249-E.

[26] S. Catani et al., Nucl. Phys. B406 (1993) 187;
S. Catani, Yu.L. Dokshitzer and B. R. Webber, Phys. Lett. B285 (1992) 291.

[27] A similar procedure was used in Monte Carlo studies as a way to select resolved events: A. Valkarova, Proceedings of the Workshop "Physics at HERA", Hamburg 1991, p. 535.

[28] G. D'Agostini, DESY 94-099 (1994).

[29] M. Basile et al., Nuovo Cim. 79 A (1984) 1.

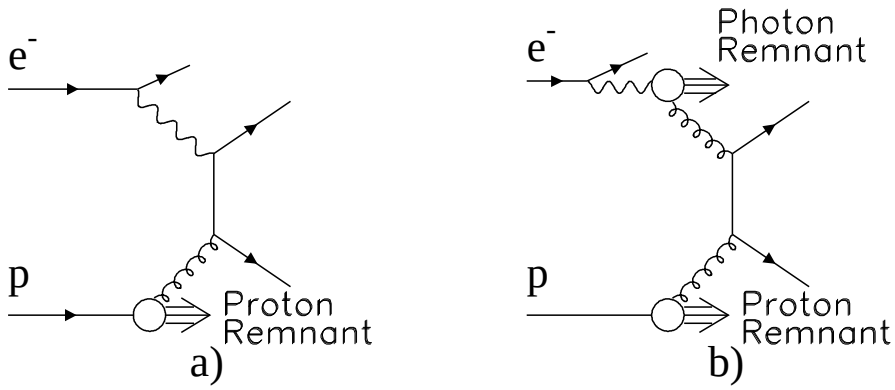

Figure 1: Examples of leading order diagrams for (a) direct and (b) resolved hard photoproduction interactions.

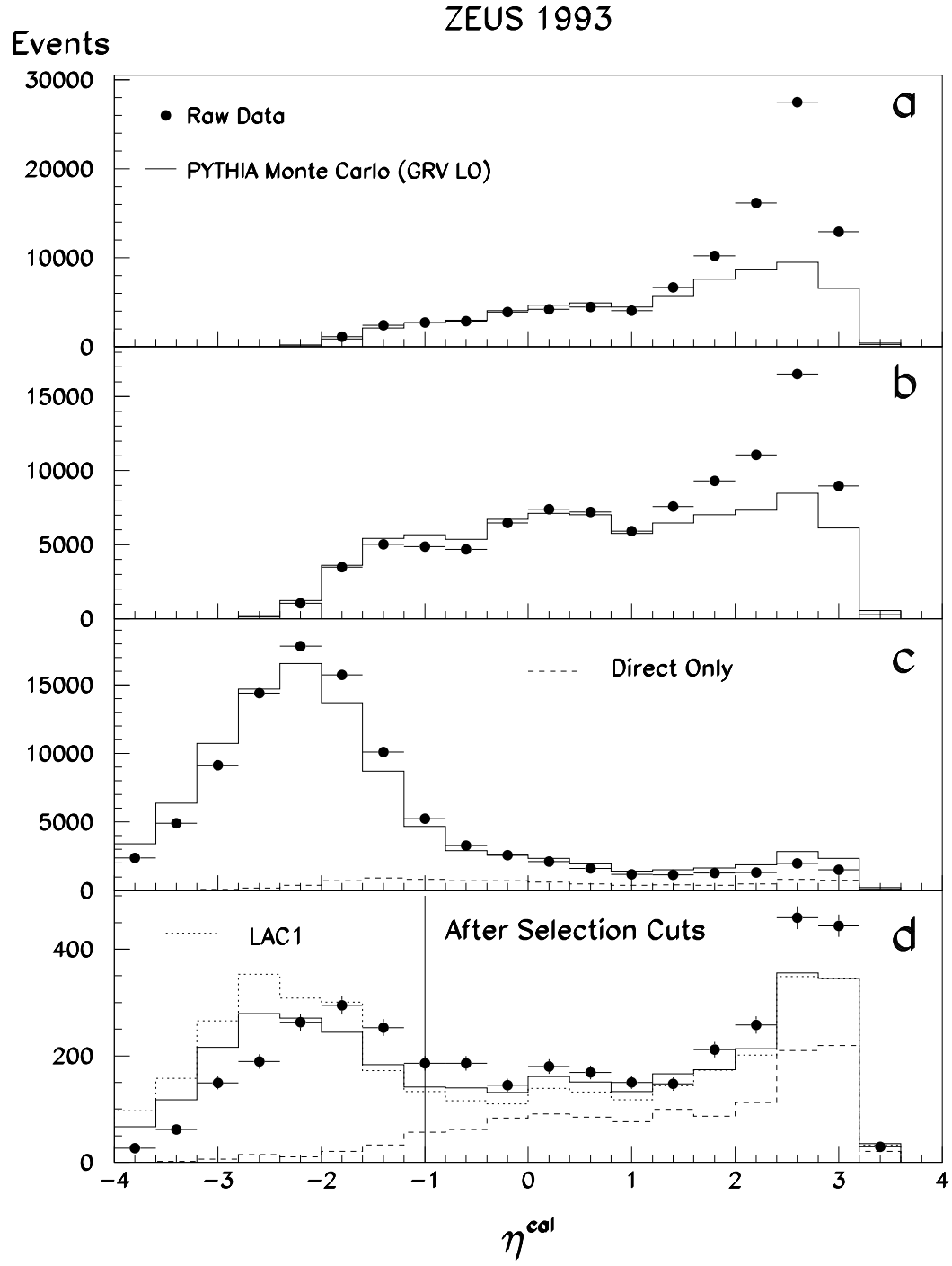

Figure 2: Pseudorapidity distributions of clusters for the inclusive photoproduction sample. The three clusters are sorted by ${p_T}^{cal}$ with (a) having the highest, (b) the second highest, and (c) the lowest ${p_T}^{cal}$. Each Monte Carlo distribution is independently normalized to the data in the region $\eta^{cal} < 1.6$. In (c) and (d) the direct contribution alone is shown as the dashed line. The η^{cal} distribution of the lowest ${p_T}^{cal}$ cluster (as in (c)) is shown again in (d) after requiring $p_{T1,2}^{cal} > 5$ GeV, $\eta_{1,2}^{cal} < 1.6$, and $E_3^{cal} > 2$ GeV. Resolved events are selected by requiring $\eta_3^{cal} < -1$ (vertical line in (d)). The dotted line shows the expectation using the LAC1 photon parton parameterization.

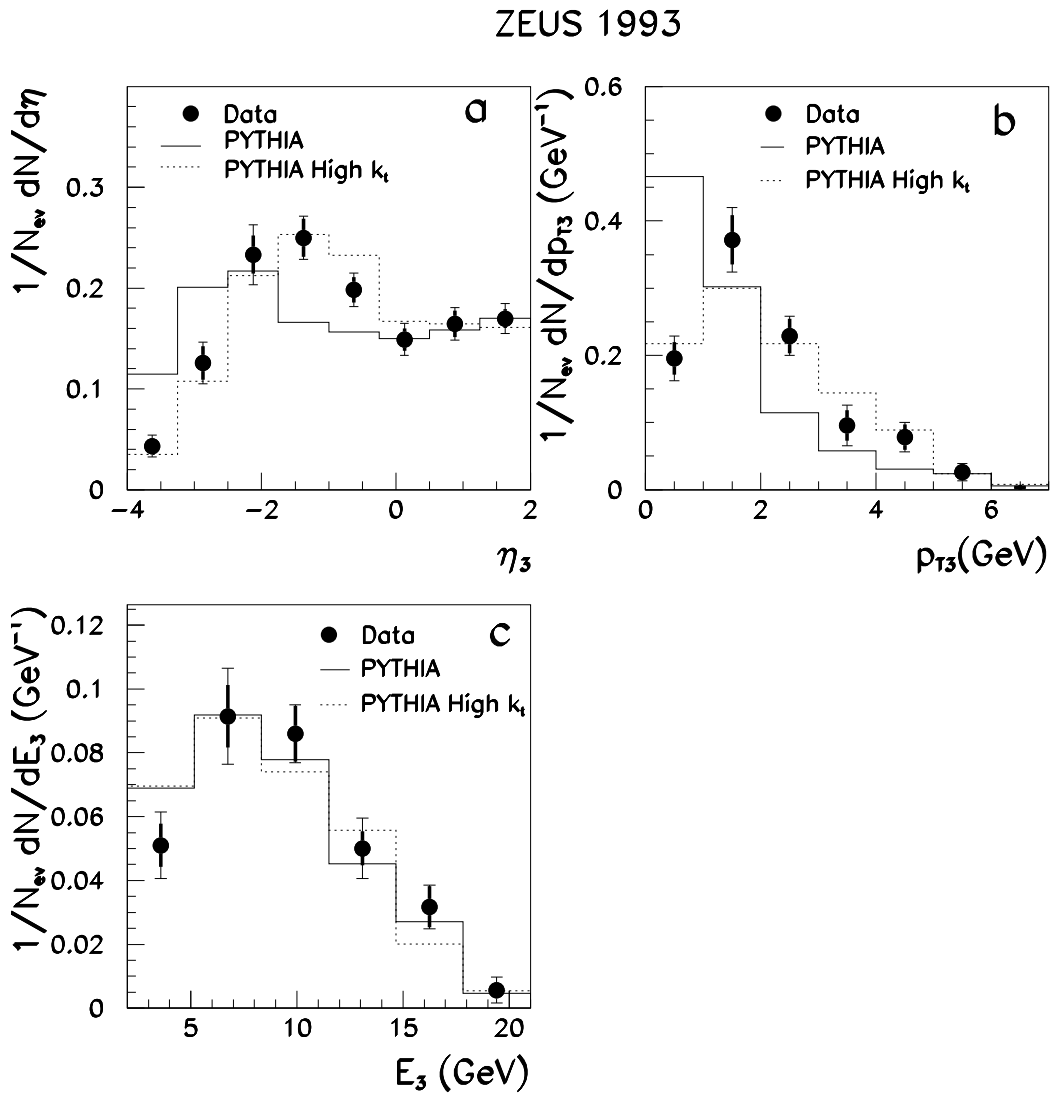

Figure 3: (a) Pseudorapidity distribution of the third cluster corrected back to the hadron level. (b) Corrected p_T distribution. (c) Corrected energy distribution. In (b) and (c) we require $\eta_3 < -1$. The solid histograms are the hadron level distributions given by the default version of PYTHIA (Gaussian with $k_0 = 0.44$ GeV). For each of the figures, the dotted line shows the Monte Carlo predictions with $dN/dk_t^2 \propto 1/(k_t^2 + k_0^2)$ and $k_0 = 0.66$ GeV, corresponding to $\langle k_t \rangle \approx 1.7$ GeV.

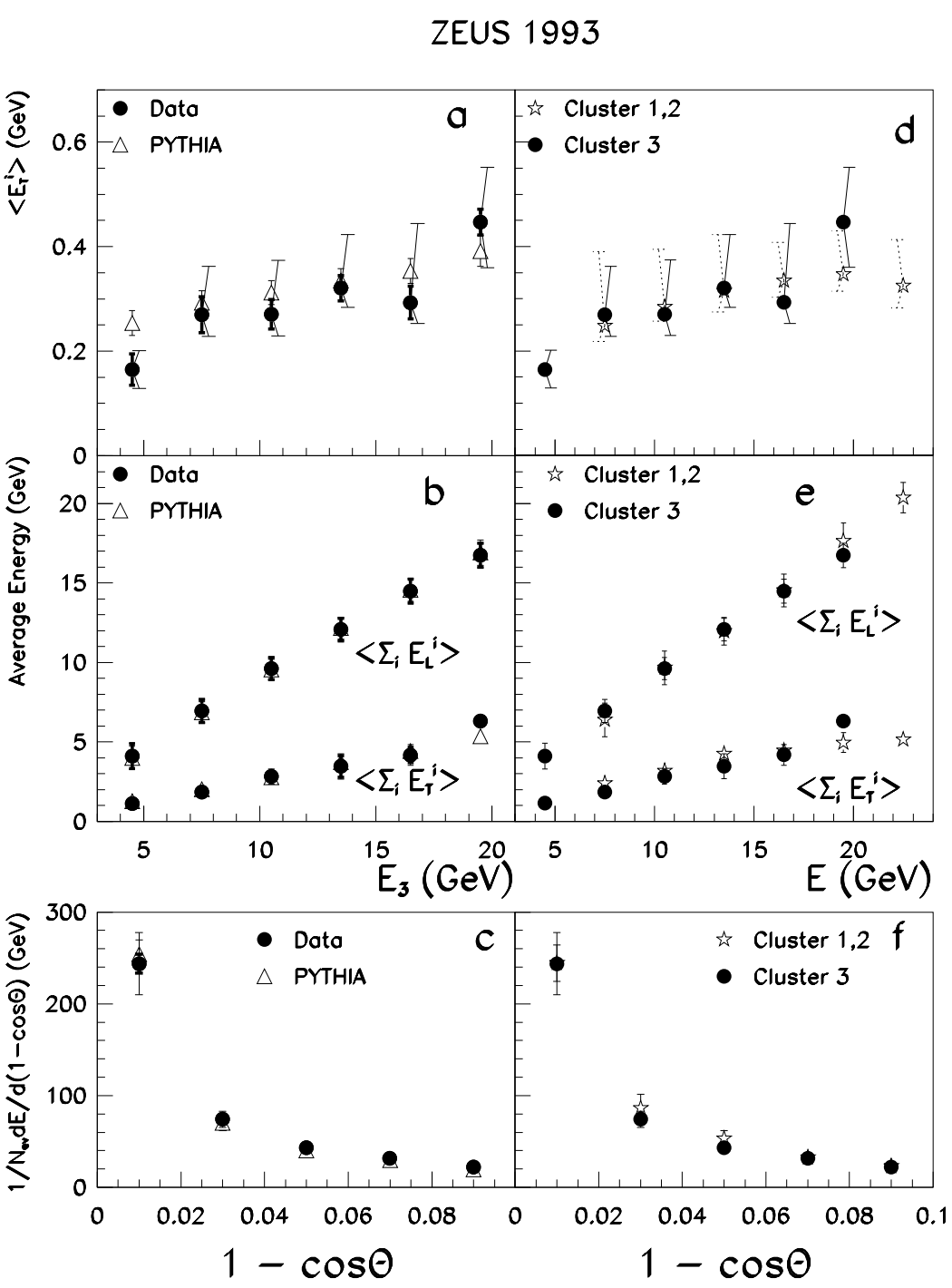

Figure 4: (a-c) Comparison between the data and the hadron level Monte Carlo expectations. (a) The mean value of $\langle E_T^i \rangle$, the average energy transverse to the cluster axis per particle, as a function of the cluster energy. (b) The average values of the total transverse ($\Sigma_i E_T^i$) and total longitudinal ($\Sigma_i E_L^i$) energy. (c) The flow of energy around the cluster axis. (d-f) Comparison between the photon remnant (cluster 3) and the two high-p_T jets. The error bars show the systematic and statistical errors added in quadrature.